



Cylindrical nano-indentation on metal film/elastic substrate system with discrete dislocation plasticity analysis: A simple model for nano-indentation size effect

Chaojun Ouyang^{a,c}, Zhenhuan Li^{a,b,*}, Minsheng Huang^{a,b}, Haidong Fan^{a,b}

^a Department of Mechanics, Huazhong University of Science and Technology, Wuhan 430074, China

^b Hubei Key Laboratory for Engineering Structural Analysis and Safety Assessment, Luoyu Road 1037, Wuhan 430074, China

^c Institute of Mountain Hazards and Environment, CAS, #.9, Block 4, Renminnanlu Road, Chengdu 610041, China

ARTICLE INFO

Article history:

Received 15 December 2009

Received in revised form 3 July 2010

Available online 23 July 2010

Keywords:

Film/substrate system

Indentation size effect

Discrete dislocation plasticity

Cylindrical indenter

Geometrically necessary dislocation

ABSTRACT

The cylindrical nano-indentation on metal film/elastic substrate is computationally studied using two-dimensional discrete dislocation plasticity combined with the commercial software ANSYS®, with a focus on the storage volume for geometrically necessary dislocations (GNDs) inside the films and the nano-indentation size effect (NISE). Our calculations show that almost all GNDs are stored in a rectangular area determined by the film thickness and the actual contact width. The variations of indentation contact width with indentation depth for various film thicknesses and indenter radii are fitted by an exponential relation, and then the GND density underneath the indenter is estimated. Based on the Taylor dislocation model and Tabor formula, a simple model for the dependence of the nano-indentation hardness of the film/substrate system on the indentation depth, the indenter radius and the film thickness is established, showing a good agreement with the present numerical results.

© 2010 Published by Elsevier Ltd.

1. Introduction

With rapid advances in micro-fabrication, the dominant size of many micro-electromechanical systems and devices is reduced to the micron and sub-micron scale by the extensive use of thin film materials. In these applications, a thorough understanding of thin film mechanical properties is very essential for successful safety design and reliability assessment of micro-systems or micro-devices.

In the past twenty years, a series of micro-experiments, such as micro-bend (Stölken and Evans, 1998), micro-tension (Espinosa et al., 2003), bulge test (Vlassak and Nix, 1992), micro-indentation (Nix, 1989) and other techniques (Voyiadjis and Deliktas, 2009), have been elaborately designed to measure the mechanical properties of thin films, either freestanding or bonded to a substrate. Compared with other micro-experiments, micro-indentation test instruments are relatively easily available and thus are extensively adopted to measure some basic mechanical properties of thin films (Nix, 1989; Zhao et al., 2007, 2008; Voyiadjis and Deliktas, 2009). However, a series of studies indicated that the factors influencing the indentation size effects are quite complex, not only depending on the indenter geometry (shape and size) (Swadener et al., 2001, 2002; Xue et al., 2002) but also on the film material properties (soft

or hard) (Saha et al., 2001; Saha and Nix, 2002). In particular, when measuring the nano/micro-indentation hardness of thin films with the thickness of only several microns or dozens of nanometers, strong constraint to the dislocation glide in thin film from elastic substrate must be considered (Joslin and Oliver, 1990; Saha et al., 2001; Saha and Nix, 2002; Chen et al., 2007). The indentation of thin films usually displays very different behaviors from bulk metals; as a result, it is extremely difficult to measure the mechanical properties of film materials (Chen et al., 2005, 2007). Some people argued that influences from the substrate can be ignored when the indentation depth is less than one tenth of the thin film thickness (Buckle, 1973); however, others claimed that this empirical rule is not always valid even for a hard film on a soft substrate (Pelletier et al., 2006). In fact, it is very difficult to insure that the indentation depth is always less than one tenth of the film thickness especially when the thickness of the thin film is on the sub-micron or nanometer order (Xu and Rowcliffe, 2004; Chen et al., 2005, 2007). Therefore, when employing nano/micro-indentation experiments to measure the mechanical properties of thin films with micron or nanometer thickness, many problems are still open for solutions (Oliver and Pharr, 2004).

In addition to nano-indentation experiments, numerical simulation has also been extensively adopted to address the above-mentioned problems. Finite element methods based on the scale-dependent continuum plasticity (Chen et al., 2007; Zhang et al., 2007; Fredriksson and Larsson, 2008) and molecular dynamics methods (Bolesta and Fomin, 2009) have been developed to model

* Corresponding author at: Department of Mechanics, Huazhong University of Science and Technology, Wuhan 430074, China. Fax: +86 27 87543501.

E-mail address: Zhli68@263.net (Z. Li).

nano/micro-indentation on the film-substrate system. Besides, discrete dislocation dynamics (DDD) is also an efficient numerical tool to capture the size effect induced by multi-mechanisms (strain gradient or non-strain gradient mechanism) at the intermediate length scale between the atomic scale and the continuum plasticity scale (Van der Giessen and Needleman, 1995; Groh and Zbib, 2009). Kreuzer and Pippan (2007) carefully analyzed the influence of the orientation of predefined slip bands on the indentation size effect. Balint et al. (2006) carried out a 2D-DDD modeling of indentation of a single crystal film bonded on a rigid substrate by a rigid wedge indenter, showing significant influences of film thickness on the transition from size-dependent hardness to size-independent continuum hardness. Widjaja et al. systematically modeled the wedge indentation on a single crystal material (Widjaja et al., 2007a) and a polycrystalline material (Widjaja et al., 2007b), investigated the size effects from indenter depth, wedge angle, as well as grain size. However, it is well known that the indenter tip in actual experiments is usually curved. To consider the effect of the tip curvature, Widjaja et al. (2005, 2007c) further analyzed the indentation of a planar single crystal by a cylindrical rigid indenter to gain insight into the indentation size effect, with an especial emphasis on the influence of the density of dislocation sources on indentation size effect. Ouyang et al. (2008) further reported a two-dimensional simulation of the nano-indentation in polycrystals using a cylindrical indenter, and revealed strong dependence of the indentation hardness on the indenter radius, grain size, indentation depth, and the distance between the grain boundary and the indenter. These works are helpful to understand dislocation mechanisms and intricate size effects of nano/micro-indentation. However, these simulations associated with cylindrical indenter do not consider the effects on indentation hardness from another important scale-film thickness.

In addition, a series of theoretical analysis have been carried out to depict the nano/micro-indentation hardness of film/substrate systems (Saha et al., 2001; Saha and Nix, 2002) and bulk materials (Nix and Gao, 1998; Swadener et al., 2001, 2002; Abu Al-Rub, 2007). Based on the assumption that all geometrically necessary dislocation loops injected by a rigid sharp conical indenter reside uniformly within a hemispherical volume scaled with the contact diameter, Nix and Gao (1998) derived a simple model linearly relating the square of micro-indentation hardness H^2 to the reciprocal of indentation depth h . Recent experiments show that this model is true for most of micro-indentation hardness data (Ma and Clarke, 1995; McElhaney et al., 1998) but overestimates the nano-indentation hardness (Lim and Chaudhri, 1999; Liu and Ngan, 2001; Feng and Nix, 2004; Elmestafa and Stone, 2002). There may be several causes contributing to this gap between the model prediction and experimental results for nano-indentation (Qiu et al., 2001; Elmestafa et al., 2004; Zhang et al., 2004), of which an overestimation of the GND density or strain gradient underneath the indenter may be the most significant one (Feng and Nix, 2004; Durst et al., 2006; Huang et al., 2006, 2007; Qin et al., 2009). Based on this viewpoint, two effective measures have been suggested to correct this overestimation of GND densities or strain gradients. One is to consider the actually existing indenter tip radius (Swadener et al., 2001, 2002; Qu et al., 2006); the other is to properly enlarge the storage volume for GNDs (Feng and Nix, 2004; Durst et al., 2006). Although these modified models give satisfactory agreement with the experimental data of nano-indentation hardness, the average GND density below the nano-indenter is unphysically high when the indentation depth is very shallow or the indenter radius is very small (Huang et al., 2006, 2007; Qin et al., 2009). For this reason, Huang et al. introduced the maximum allowable GND density to cap the excessively high GND density underneath the tip indenter (Huang et al., 2006) and the spherical indenter (Huang et al., 2007; Qin et al., 2009). As they

showed, this remedy gives good agreement with micro-indentation hardness as well as nano-indentation hardness for both the tip indenter and the spherical indenter (Huang et al., 2006, 2007; Qin et al., 2009). As is well known, all models mentioned above are based on the classical Taylor relation $\tau = \sqrt{\rho_{SSD} + \rho_{GND}}$, where the hardening law was taken as a simple linear sum of the SSD density ρ_{SSD} and GND density ρ_{GND} . Abu Al-Rub and Voyiadjis (2004) ascribed the aforementioned overestimation of nano-indentation hardness to this simple linear coupling, and suggested a nonlinear coupling between ρ_{SSD} and ρ_{GND} (i.e. $\tau = \sqrt[3]{\rho_{SSD}^3 + \rho_{GND}^3}$), to improve the model prediction of nano-indentation hardness for sharp indenters as well as spherical indenters. Comparison between model prediction and the measured nano-indentation hardness data showed that their model can successfully predict the nano/micro-hardness data for spherical and pyramidal indenters. Obviously, although these methods are different, the central idea is to depict rationally the hardening law of the materials underneath the nano-indenter. Two measures are taken to do this. One is to estimate rationally the GND density (Feng and Nix, 2004; Durst et al., 2006; Huang et al., 2006, 2007; Qin et al., 2009) and the other is to consider rationally the complex interaction between the GNDs and SSDs (Abu Al-Rub and Voyiadjis, 2004). For the metal film-elastic substrate system, due to strong constraint to dislocation glide from the pure elastic substrate, the GND distribution zone in thin films is significantly different from that in bulk materials, so correctly determining the GND distribution zone and reliably estimating the GND density in the thin film are of vital importance for the development of a rational model to predict the nano-indentation hardness. To the best of our knowledge, this question is still open. This motivates us to carry out the present 2D discrete dislocation plasticity (DDP) analysis of cylindrical nano-indentation on metal film/elastic substrate systems, with a focus on two key points, i.e. the GND storage volume and the GND density. Based on these, a simple model for the nano-indentation size effect is suggested, which correlates the nano-indentation hardness with the indenter radius, indentation depth and thin film thickness.

2. Computational method and model

Fig. 1 illustrates the essential details of the computational model, which mainly consists of three parts, i.e. a cylindrical indenter, a metal thin film and a finite but large enough elastic substrate with length $L_1 = 1000 \mu\text{m}$ and width $L_2 = 500 \mu\text{m}$. For convenience, the origin of the coordinate system is located at the center of the upper surface of the thin film.

For the sake of simplicity, only 2D plane strain is considered, and the metal film is assumed to be perfectly bonded to the substrate. The metal film is assumed to be elasto-plastic and the substrate purely elastic, but they possess the same elastic constants with Young's module $E = 70 \text{ GPa}$ and the Poisson's ratio $\nu = 0.3$. As is well known, the plastic deformation of the metal generally roots in the collective motion and the dynamic evolution of dislocations. Based on this fundamental knowledge, in the DDP framework, the plastic deformation of the metal can be modeled by dynamically tracking the motion and evolution of individual dislocations. To model the plastic deformation within the film, some potentially activated slip planes with a specified separation distance are pre-arranged within the film and some dislocation sources are randomly dispersed on these potential slip planes. Under enough resolved shear stress, some dislocations can nucleate from these dislocation sources and glide on their own slip plane; as a result, the plastic deformation occurs. Therefore, the soul of DDP lies in how to track dynamically the motion and evolution of individual dislocations as mentioned below. Widjaja et al. (2005) performed 2D-DD calculations of indentation of a single crystal by a circular rigid indenter, where three slip

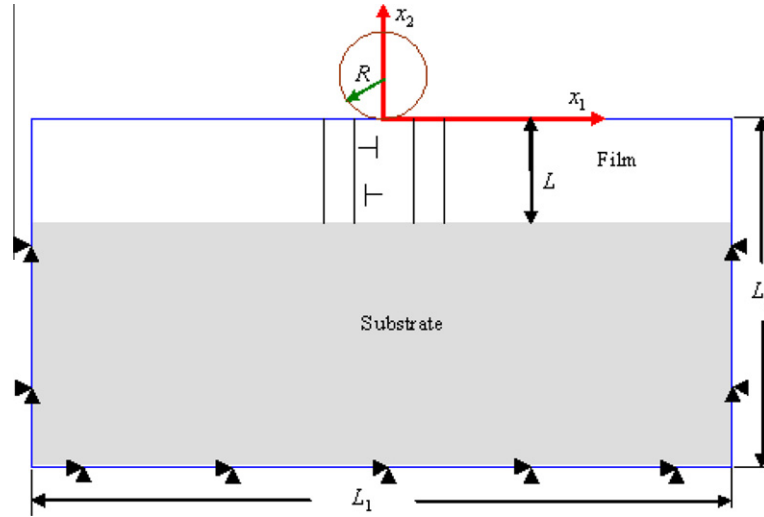


Fig. 1. Sketch of computational model for cylindrical indentation on film/substrate system.

systems oriented at 30°, 90° and 150° from the free surface are considered. Their results indicated that “the step in the surface profile due to localized slip on a 90° slip plane” (Widjaja et al., 2005). On the other hand, since the slip planes in a direction parallel to the cylinder loading direction have major contributions to the geometrically necessary dislocations (GNDs), only single slip system oriented at 90° from the free surface is considered in our model for simplification. The magnitude of the Burgers vector is typically chosen as $b = 0.25$ nm and the distance between two adjacent potentially activated slip planes is typically set to be $100b$. No initial dislocations exist in the film but some Frank–Read sources with a given source density $\rho_{sou} = 240 \mu\text{m}^{-2}$ randomly distribute on potentially activated slip planes. Such high dislocation source density is adopted mainly for the following reasons. In our computation, only the nano-indentation of cylindrical indenter is modeled. The indentation-affected zone under the indenter is such small that only few dislocations can nucleate and glide there if a relatively lower dislocation source density is given. As a result, the randomness of the computed indentation force and hardness increases largely, rendering great difficulty in analysis of computational results. Indeed, the dislocation source density of $\rho_{sou} = 240 \mu\text{m}^{-2}$ is much higher than what has been frequently used in the previous DDD simulations of indentation (Widjaja et al., 2007c) but still substantially below the densities used by Kreuzer and Pippan (2004, 2007).

During initial phase of indenting, due to the lack of dislocations, the stress and strain fields in the film and elastic substrate can be easily solved by the linearly elastic finite element method. With the increase of indentation depth, two opposite-signed dislocations with a critical interval of $6b$ nucleate from the Frank–Read source once the resolved shear stress τ acting on the Frank–Read source goes beyond the critical nucleation strength τ_{nuc} . Here τ_{nuc} is typically assumed to follow a Gaussian distribution with an average $\bar{\tau}_{nuc} = 50$ MPa and a standard deviation $s = 1$ MPa. Once dislocations appear in the thin film, the singular elastic field of dislocations should be considered. Theoretically speaking, the total deformation field $(\mathbf{u}, \mathbf{\varepsilon}, \boldsymbol{\sigma})$ in the thin film should be the superposition of the smooth image field $(\hat{\mathbf{u}}, \hat{\mathbf{\varepsilon}}, \hat{\boldsymbol{\sigma}})$ induced by the model boundary condition and the singular field $(\tilde{\mathbf{u}}, \tilde{\mathbf{\varepsilon}}, \tilde{\boldsymbol{\sigma}})$ induced by individual dislocations, as suggested by Van der Giessen and Needleman (1995):

$$\mathbf{u} = \hat{\mathbf{u}} + \tilde{\mathbf{u}}; \quad \mathbf{\varepsilon} = \hat{\mathbf{\varepsilon}} + \tilde{\mathbf{\varepsilon}}; \quad \boldsymbol{\sigma} = \hat{\boldsymbol{\sigma}} + \tilde{\boldsymbol{\sigma}}. \quad (1)$$

As is well known, dislocation can be considered as a typical line defect. Therefore, its evolution is firmly controlled by the so-called configurational force or Peach–Koehler force (Van der Giessen and Needleman, 1995).

$$f^{(j)} = \mathbf{m}^{(j)} \cdot \left(\hat{\boldsymbol{\sigma}} + \sum_{K \neq j} \boldsymbol{\sigma}^{(K)} \right) \cdot \mathbf{b}^{(j)}, \quad (2)$$

where $\boldsymbol{\sigma}^{(K)}$ is the contribution from the dislocation K to the Peach–Koehler force $f^{(j)}$ acting on the dislocation J , $\mathbf{b}^{(j)}$ is the Burgers vector of dislocation J ; and $\mathbf{m}^{(j)}$ is the normal vector of the slip plane on which the dislocation J is located.

Besides, a series of dislocation short-range interactions are also considered, such as dislocation annihilation between two opposite-signed dislocations. A slip step is left at the surface of the film when a dislocation slips out of it. On the other hand, dislocations pile up when they approach the interface between the film and the substrate. Within each loading increment, a dislocation stops at its equilibrium position if the Peach–Koehler force f acting on it is less than the lattice friction τ_f approximatively set as 2 MPa (Olmsted et al., 2001). Only when all dislocations stop in their respective equilibrium positions, is a new loading increment applied and the indenter continues to move down until it reaches the required indentation depth. More details can be found from the literature (Van der Giessen and Needleman, 1995; Widjaja et al., 2005, 2007a,b,c; Balint et al., 2006; Kreuzer and Pippan, 2007; Ouyang et al., 2008).

Since plastic flow is mainly confined to the thin film, the displacement conditions on the lower, left and right boundaries of the computational model can be assumed as:

$$\dot{u}_1 = \dot{u}_2 = 0, \quad \text{on } x_1 = \pm L_1/2 \quad \text{and } x_2 = -L_2. \quad (3)$$

At the upper surface of the thin film, the portion not in contact with the indenter is traction free:

$$\dot{T}_1 = \dot{T}_2 = 0 \quad \text{on } x_2 = 0 \notin S_c, \quad (4)$$

where $T_i = \sigma_{ij}n_j$ is the traction on the surface with an outward normal n_j and S_c is the contact area between the indenter and the film. Lagrange contact algorithm provided by ANSYS® is used to deal with dynamic contact between the cylindrical indenter and the thin film.

In all calculations, the loading is applied with a controlled indenter displacement of $\Delta\delta = 0.05$ nm in each time step.

The indentation force applied on the indenter is calculated by

$$F = - \int_{S_c} T_2(x_2, h) dx_1. \quad (5)$$

The relation between the indentation hardness and the indentation force can be expressed as:

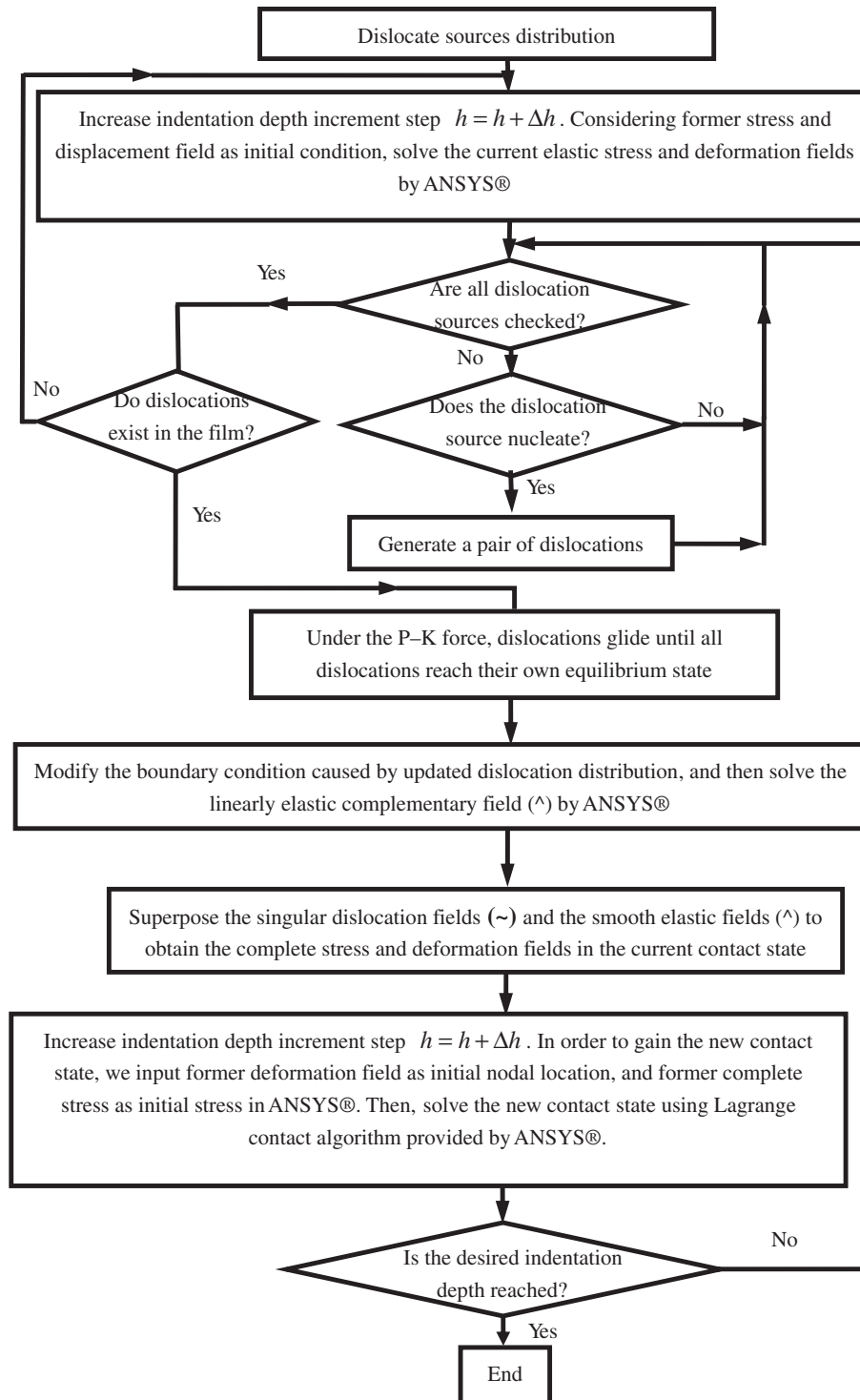
$$H = F/a_c, \quad (6)$$

where a_c is the actual contact area (the contact width for the present 2D case) between the indenter and the film, which takes into account roughening of the top surface after the dislocations have left the materials as shown in Fig. 5. In order to accurately capture the contact width a_c , the finite element meshes are refined at the zone underneath the indenter and the minimal mesh size is about $0.006 \mu\text{m}$.

The computational flow chart adopted is given as follows:

3. Results and discussions

The indentation force F and hardness H are plotted as functions of the indentation depth h in Fig. 2(a) and (b), respectively, for five thin film thicknesses, where the cylindrical indenter radius is typically taken as $R = 2 \mu\text{m}$. It can be clearly seen from Fig. 2(a) and (b) that the indentation force F and hardness H strongly depend on the film thickness L , especially when h is large, say $h > 0.03 \mu\text{m}$, and the



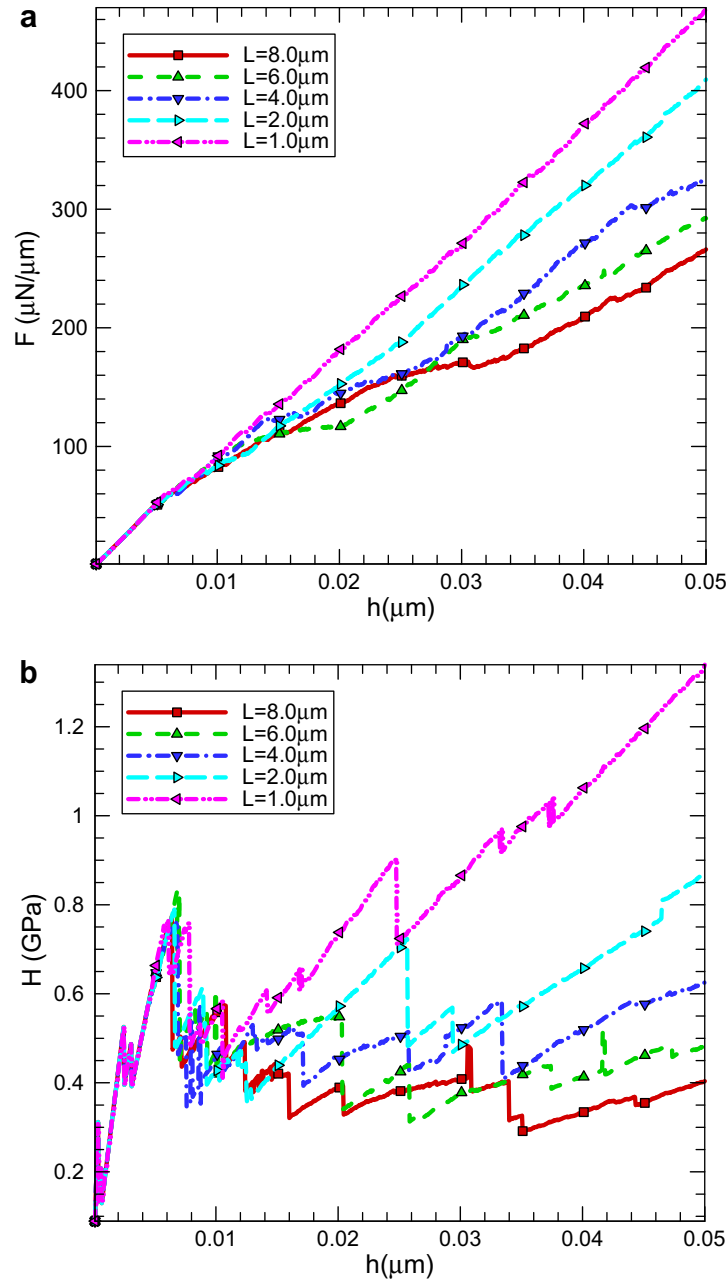


Fig. 2. Influences of film thickness on (a) F - h curves and (b) H - h curves for given indenter radius $R = 2.0 \mu\text{m}$.

film thickness L small, say $L < 4 \mu\text{m}$. These results can be ascribed to two main reasons. First, in thin films, nucleated dislocations can be more easily blocked and pile up at the film-substrate interface. With more and more dislocations piling up at the film-substrate interface, back stress from these dislocation pile-ups imposes strong reaction against subsequent dislocation nucleating and dislocation gliding, and the result is that the plastic deformation becomes more and more difficult. Second, when the film thickness is small, the number of dislocation sources underneath the indenter is relatively small, so plastic deformation can hardly occur. Therefore, plastic deformation becomes more and more difficult with the decrease of film thickness, and to accommodate the applied indentation depth, a higher indentation force F is required; as a result, the indentation hardness H clearly increases. In addition, it can be seen from Fig. 2(a) and (b) that the indentation force F and hardness H are almost independent of the film thickness

L when the indentation depth h is small, say $h < 0.01 \mu\text{m}$. With the indentation depth gradually increasing, the influence of the thin film thickness L on the indentation force F and hardness H becomes more and more strong. It deserves to be especially noted that the F - h curves begin to leave each other at $h \approx 0.01 \mu\text{m} \leq L/10$ for two thinner films with thickness $L = 1 \mu\text{m}$, $2 \mu\text{m}$ and at $h \approx 0.03 \mu\text{m} \leq L/10$ for thicker films with thickness $L \geq 4 \mu\text{m}$. It follows that for all thin film thicknesses considered, as long as plastic deformation occurs, the indentation force F and hardness H strongly depend on the thin film thickness L even when $h < L/10$. Obviously, the well-known empirical rule for film hardness measurement, which says that the indentation depth should be smaller than one tenth of the film thickness to avoid substrate effects, seems unsuitable. This conclusion is consistent with results in published literatures (Chen et al., 2005, 2007; Pelletier et al., 2006; Xu and Rowcliffe, 2004)).

Fig. 3 shows the influence of the thin film thickness L on the variation of the actual contact width a_c between the film and the indenter with an indentation depth h , for one randomly chosen indenter radius of $R = 2 \mu\text{m}$. It is clearly seen that there are some steps in all plastic a_c – h curves, indicating that intermittent contact happens between the indenter and the film due to more slip steps appearing on the contact interface. In addition, once plastic deformation happens in the thin film (corresponding to $h > 0.006 \mu\text{m}$), the influence of the thin film thickness L on the actual contact width a_c becomes stronger and stronger with the increase of the indentation depth h .

In order to clearly understand the underlying mechanism leading to the results mentioned above, Fig. 4 depicts the dislocation pattern and distribution of the slip quantity $I' = |\gamma^{\phi=90^\circ}| = |s_i e_{ij} m_j|$ in the films with different thicknesses, here s_i and m_j are the tangential and normal vectors of the slip system ϕ , respectively. In thinner films like $L = 1.0 \mu\text{m}$ shown in Fig. 4(a), due to strong obstacle from the film-substrate interface, some dislocations pile up at the film-substrate interface and impose strong reaction to dislocation sources and moving dislocations; on the other hand, the dislocation mean slip path is shorter in thinner films, so plastic deformation is more hardly to occur. To accommodate the applied indentation depth, some dislocations must nucleate from those sources on those slip planes far from the central plane of the indenter. This means that dislocations in the thinner film are distributed in a relatively dispersed manner. As a result, more but shallower slip steps occur on the surface of thinner films, and the curvature of indentation is relatively smaller. However, in thicker films like $L = 8.0 \mu\text{m}$ shown in Fig. 4(d), since the mean slip path of dislocations is longer and the constraint from the film-substrate interface is relatively weaker than those in thinner films, almost all dislocations are distributed within a band zone underneath the indenter and almost no dislocations nucleate and glide on those slip planes far from the indenter central plane. Due to relatively highly centralized slip in the thicker film, the number of activated slip planes is smaller but the slip quantity is relatively larger. Compared with the slip step and the curvature of indentation on the surface of thinner films, the slip steps present on the surface of thicker films is relatively deeper and the curvature of indentation is relatively larger. As a result, at the same indentation depth, the width (i.e.

length for the present 2D case) of the contact area between indentation and the film for thinner films is shorter than that for thicker films as shown in Fig. 4 and sketched in Fig. 5. Careful examination of dislocation distribution patterns in thinner films as shown in Fig. 4(a) indicates that, although some dislocations are distributed on those slip planes far from the central plane of the indenter, most of them are opposite-signed dislocation pairs and only few GND are present, i.e., most of GNDs still reside within a rectangular area right below the indentation. By careful comparison of Fig. 4(a)–(d), it can be seen that, for the same indenter radius and at the same indentation depth, most of GNDs are located right below the indentation and reside within a rectangular area with length a_c and width L for both thinner films and thicker films.

Based on the discussions above, it can be seen that nano-indentation hardness strongly depends on the film thickness. As pointed out by Swadener et al. (2001, 2002), hardness depends on the diameter of the indenter rather than on the depth of the indentation for the spherical indenter. In order to measure conveniently the nano-indentation hardness of film-substrate systems, it is necessary to establish a simple model which includes indentation size effects and relates indentation hardness H to the film thickness L , indenter radius R and contact width a_c . The central issue is how to rationally estimate the GND density ρ_{GND} , which is closely related to the number of GNDs (N_{GND}) and the area of the GND distribution zone (A_{GND}). At present, there still exist some disagreements on this issue (Nix and Gao, 1998; Swadener et al., 2001, 2002; Feng and Nix, 2004; Abu Al-Rub and Voyiadjis, 2004; Durst et al., 2006; Huang et al., 2006, 2007; Qin et al., 2009).

Considering the assumption of Nix–Gao model that all GNDs are stored in a hemisphere of radius a_c does not hold in nano-indentation, some models were suggested to extend storage volume for GNDs (Feng and Nix, 2004; Huang et al., 2006, 2007). For the present nano-indentation of the film-substrate system by a circular rigid indenter, as shown in Fig. 4, most of GNDs reside in a rectangular zone with length a_c and width L , which is larger than a hemispherical zone with a diameter a_c assumed by Nix and Gao (1998) for the micro-indentation of a bulk material by a wedge indenter. Hence, the area of the GND distribution zone can be approximately expressed as:

$$A_{\text{GND}} = a_c L. \quad (7)$$

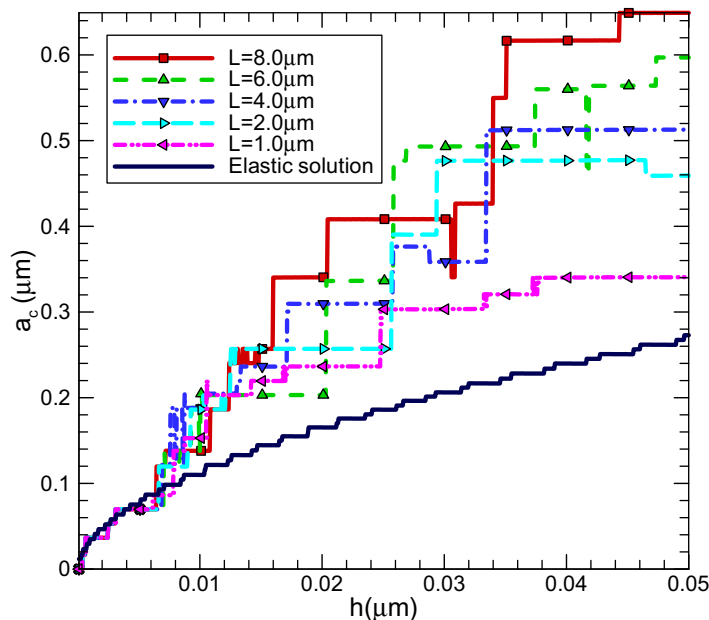


Fig. 3. Influences of film thickness on a_c – h curves for given indenter radius $R = 2.0 \mu\text{m}$, where the curve for pure elastic indentation is given.

Similar to Nix and Gao (1998) and Swadener et al. (2001, 2002), the number of GNDs can be formulated as:

$$N_{GND} = \frac{2h_c}{b} = \frac{a_c^2}{Rb}, \quad (8)$$

where h_c is the actual indentation depth corresponding to the actual contact width a_c . The present calculations show that Eq. (8) can give

a satisfactory estimation of the number of GNDs underneath the indenters with various radii.

According to Eqs. (7) and (8), for the present 2D cases, the GND density ρ_{GND} underneath the indenter can be further approximated as:

$$\rho_{GND} = \frac{N_{GND}}{A_{GND}} = \frac{a_c}{RLb}. \quad (9)$$

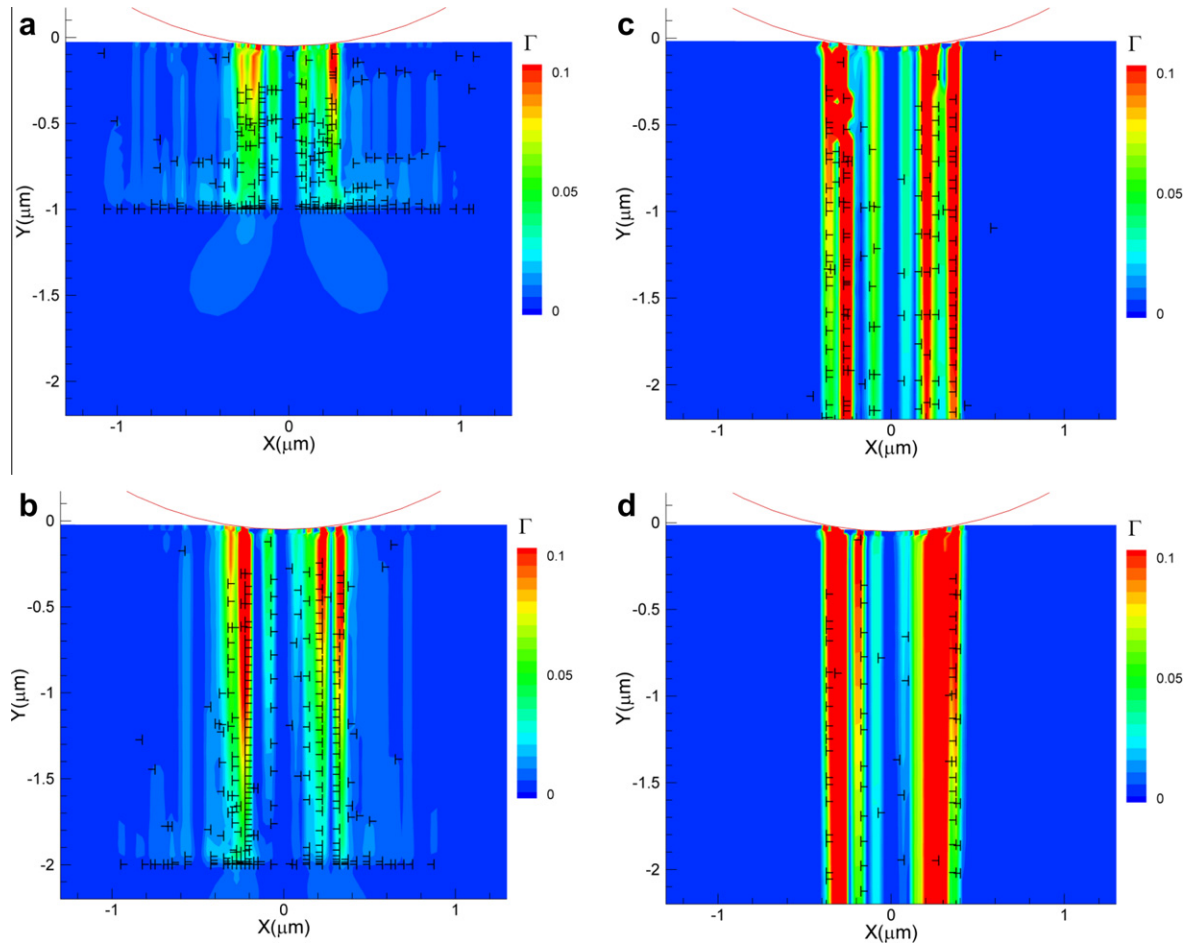


Fig. 4. Dislocation pattern and distribution slip quantity Γ in the film with different thicknesses: (a) $L = 1.0 \mu\text{m}$; (b) $L = 2.0 \mu\text{m}$; (c) $L = 4.0 \mu\text{m}$; (d) $L = 8 \mu\text{m}$ at given indentation depth $h = 0.05 \mu\text{m}$.

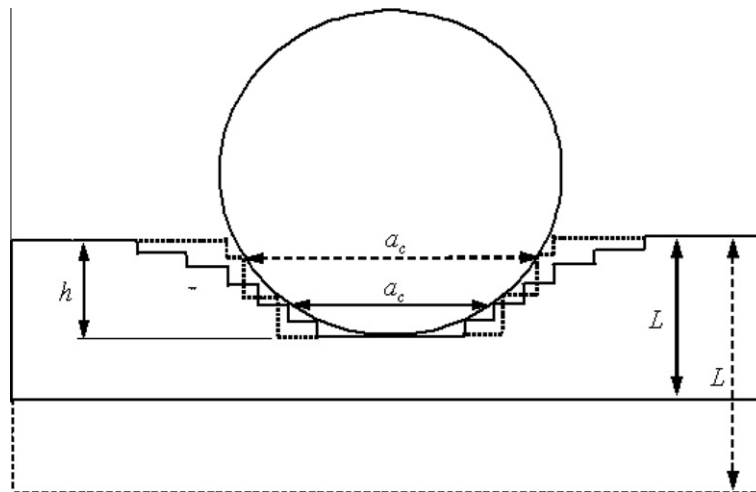


Fig. 5. Sketch for correlation between the slip steps on film surface and the diameter of actual contact area for thin film (solid line) and thick film (dash line).

As we know, the force between two parallel dislocations can be written as $\tau = \beta\mu b/(2\pi d)$, where d is the averaged distance between two dislocations. Although the dislocation spacing in a pile up is not uniform and the spacing between slip planes is not the same as the spacing between dislocations on slip planes within the rectangular indentation-affected zone, we can approximately assume $d \propto \sqrt{\rho}$. Therefore, $\tau \propto \beta\mu b\sqrt{\rho}/(2\pi) = \alpha\mu b\sqrt{\rho}$, which is similar in form to the Taylor relation. Generally speaking, the Taylor relation is suitable for forest hardening. Here, it is borrowed to describe approximately long-range hardening between parallel dislocations.

Substituting Eq. (9) into the $\tau = \alpha\mu b\sqrt{\rho_{SSD} + \bar{r}\rho_{GND}}$ and Tabor formula $H \approx 3\sigma = 3\sqrt{3}\tau$ yields

$$H = H_0 \sqrt{1 + t^* \frac{a_c}{RL}}, \quad (10)$$

where ρ_{SSD} is the density of statistically stored dislocations, $t^* = \bar{r}/(b\rho_{SSD})$, \bar{r} is the Nye factor (Arsenlis and Parks, 1999) and $H_0 = 3\sqrt{3}\alpha\mu b\sqrt{\rho_{SSD}}$.

In order to confirm whether Eq. (10) can rationally describe the size effect of nano-indentation hardness in different cases, we consider five indenter radii $R = 2, 4, 6, 8, 12 \mu\text{m}$, five film thicknesses $L = 1, 2, 4, 6, 8 \mu\text{m}$, and three random distributions of dislocation sources in each case. For all the considered cases, the variations of H^2 with a_c/R and a_c/L are plotted in Fig. 6(a) and (b), respectively. It is clear at a glance of Fig. 6(a) and (b) that H^2 indeed linearly depends on a_c/R and a_c/L , with $H_0 \approx 0.134\text{--}0.155 \text{ GPa}$ and $t^* \approx 100 \mu\text{m}$, indicating that Eq. (10) can satisfactorily depict the dependence of nano-indentation hardness H on the thin film thickness L , film/indenter contact width a_c and indenter radius R .

Due to the difficulty in experimentally measuring the actual film/indenter contact width a_c , it is necessary to establish a relationship between the contact width a_c and the thin film thickness L , indenter radius R and indentation depth h . For this purpose, the variations of a_c with R and L are plotted in Fig. 7(a) and (b), respectively. From Fig. 7(a) and (b), it can be seen that all computed data points can be well fitted by an exponential function $a_c = AR^\alpha L^\beta$ as

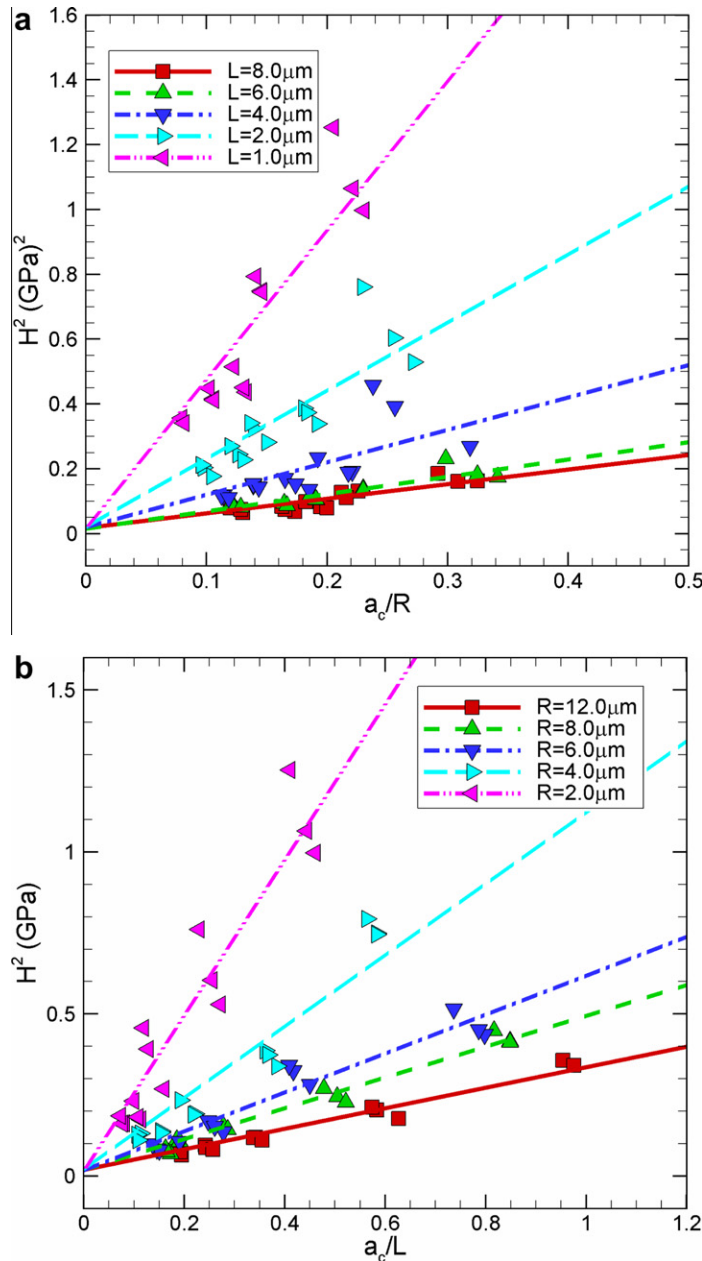


Fig. 6. The variations of the square of indentation hardness H^2 with (a) a_c/R and (b) a_c/L .

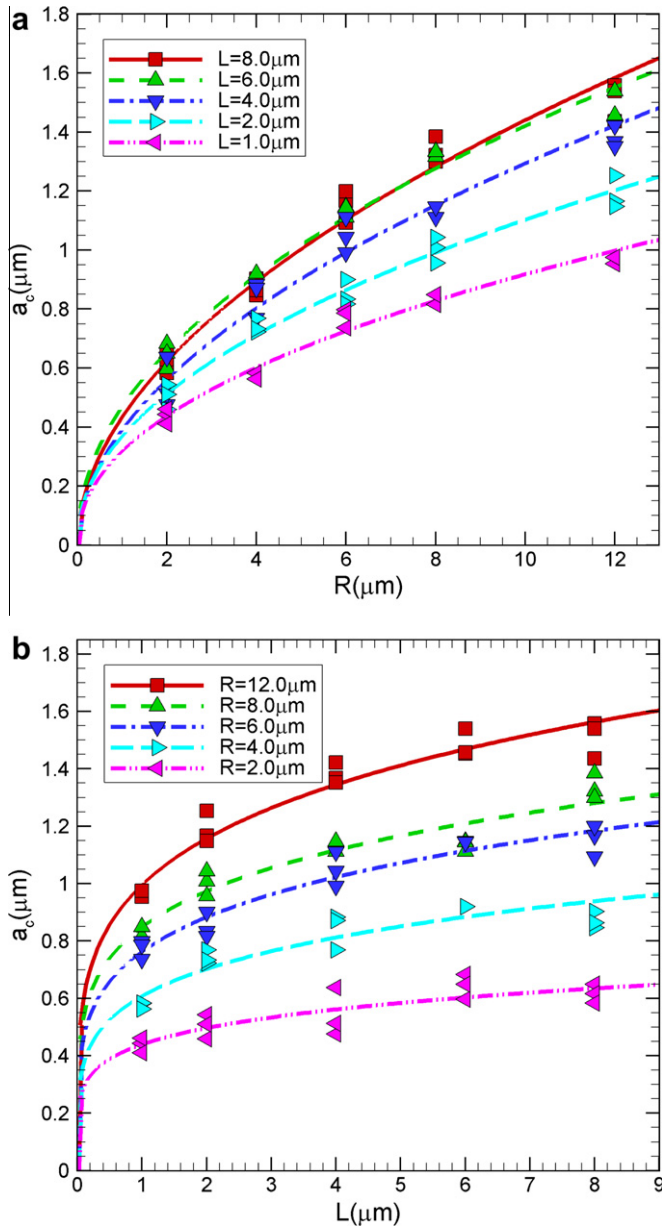


Fig. 7. The variations of actual contact diameter a_c with (a) indenter radius R and (b) film thickness L .

shown by the fitted curves. On the other hand, for simple pure elastic indentation on the present film-substrate system, the actual contact width a_c can be related to the indenter radius R and indentation depth h . For this purpose, we perform a pure elastic indentation simulation of the elastic film-elastic substrate system. Our simulation shows that for pure elastic indentation, the contact width a_c can be well fitted by $a_c^e = 2c\sqrt{Rh/2\pi}$ with $c = 1.1$, as shown in Fig. 8. Based on an overall consideration of pure elastic and elasto-plastic indentation results as shown in Figs. 7 and 8, we assume that the actual film/indenter contact width a_c can be approximated as:

$$a_c = 2c\sqrt{Rh/2\pi}\left(\frac{L}{L_0}\right)^\beta = 2.2\sqrt{Rh/2\pi}\left(\frac{L}{L_0}\right)^\beta, \quad (11)$$

where L_0 is a reference length. Obviously, when $L \rightarrow L_0$, $a_c \rightarrow a_c^e = 2.2\sqrt{Rh/2\pi}$. In the following, $L_0 \approx 0.062 \mu\text{m}$ is a good fitted value for all cases considered. This seems reasonable since when the film thickness $L \rightarrow L_0 \approx 0.062 \mu\text{m}$, it is difficult for dislocations to nucleate and glide in the film due to strong constraints from

the elastic substrate and indenter; as a result, only elastic deformation can happen, and $a_c \rightarrow a_c^e = 2.2\sqrt{Rh/2\pi}$. Therefore, Eq. (10) can be further written as:

$$a_c = \begin{cases} 2c\sqrt{Rh/2\pi}\left(\frac{L}{L_0}\right)^\beta & L \geq L_0, \\ 2c\sqrt{Rh/2\pi}, & L < L_0. \end{cases} \quad (12)$$

In order to calibrate the unknown parameters β and L_0 , we take logarithms on both sides of Eq. (11) to obtain

$$\ln\left(\frac{a_c}{2.2\sqrt{Rh/2\pi}}\right) = \beta \ln(L) - \beta \ln(L_0). \quad (13)$$

Obviously, if Eq. (11) is reasonable, $\ln\left(\frac{a_c}{2.2\sqrt{Rh/2\pi}}\right)$ should be a linear function of $\ln(L)$, with a slope β and an intercept $-\beta \ln(L_0)$. For all considered cases, including three indentation depths $h = 0.03, 0.04, 0.05 \mu\text{m}$, five indenter radii $R = 2, 4, 6, 8, 12 \mu\text{m}$, five thin film thicknesses $L = 1, 2, 4, 6, 8 \mu\text{m}$ and their combinations, the variations of $\ln\left(\frac{a_c}{2.2\sqrt{Rh/2\pi}}\right)$ with $\ln(L)$ are plotted in Fig. 9. As expected, a linear relation can be used to fit computed data points, with a slope $\beta \approx 0.18$ and an intercept $-\beta \ln(L_0) \approx 0.46$ (i.e. $L_0 \approx 0.062 \mu\text{m}$).

Substituting Eq. (11) into Eq. (10) yields

$$H = H_0 \sqrt{1 + \frac{2.2t^*}{L} \sqrt{\frac{1}{2\pi}} \sqrt{\frac{h}{R}} \left(\frac{L}{L_0}\right)^\beta} \quad L > L_0, \quad (14a)$$

or

$$\left(\frac{H}{H_0}\right)^2 = 1 + \frac{2.2t^*}{L} \sqrt{\frac{1}{2\pi}} \sqrt{\frac{h}{R}} \left(\frac{L}{L_0}\right)^\beta \quad L > L_0. \quad (14b)$$

Obviously, for the cylindrical nano-indentation on film/substrate systems, the present empirical model suggests that nano-indentation hardness H increases with the decrease of the indenter radius R and film thickness L , but decreases with the decrease of the indentation depth h . This “reverse” size dependence of H on indentation depth h seems abnormal, but is consistent with the indentation size effect for spherical indenters (Swadener et al., 2001, 2002).

In order to further validate the present empirical model, the square of the nano-hardness H^2 at an indentation depth $h = 0.05 \mu\text{m}$ is plotted as a function of $1/\sqrt{R}$ and $1/L^{1-\beta}$ ($\beta = 0.18$) in Fig. 10(a) and (b), respectively. Clearly, H^2 indeed is linearly dependent on $1/\sqrt{R}$ and $1/L^{1-\beta}$ with the same H_0 , t^* and h as fitted values in Fig. 6, i.e. $H_0 \approx 0.134\text{--}0.155 \text{ GPa}$ and $t^* \approx 100 \mu\text{m}$. This means that the present empirical model (14) can well depict the dependence of the indentation hardness H on the indenter radius R , indentation depth h and thin film thickness L .

4. Conclusions and concise remarks

In the present manuscript, the two-dimensional discrete dislocation plasticity by Van der Giessen–Needleman and the commercial finite element software ANSYS® are jointly used to analyze cylindrical nano-indentation on metal film/elastic substrate systems, with a focus on the nano-indentation size effect and underlying dislocation mechanisms. From our calculations, some results are obtained as follows:

- (1) Due to strong constraint from the elastic substrate, at the same indentation depth h , the indentation force F significantly increases with the decrease of the thin film thickness. Even when the indentation depth is smaller than one tenth of the thin film thickness i.e. $h < L/10$, the thickness L of the thin film still strongly influences the indentation force F , indicating the constraint from the elastic thin film still cannot be ignored.

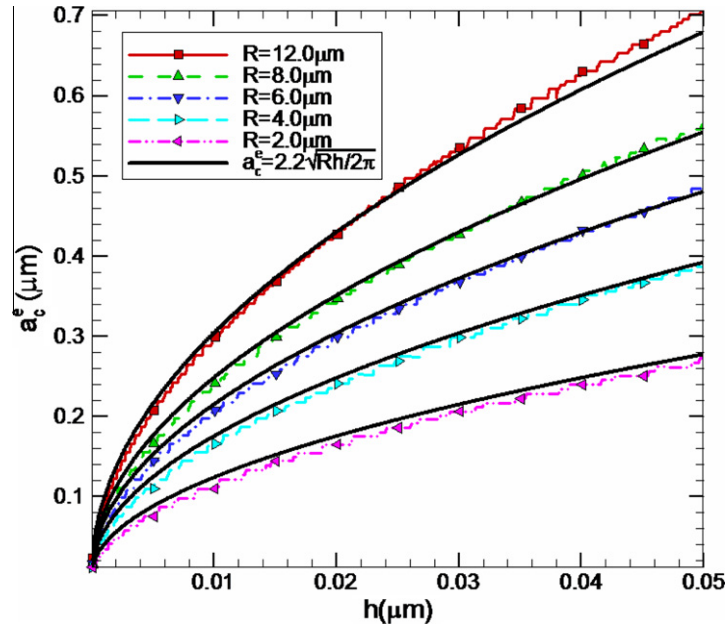


Fig. 8. The influence of indenter radius R on the dependence of elastic contact width a_c^e on elastic indentation depth h .

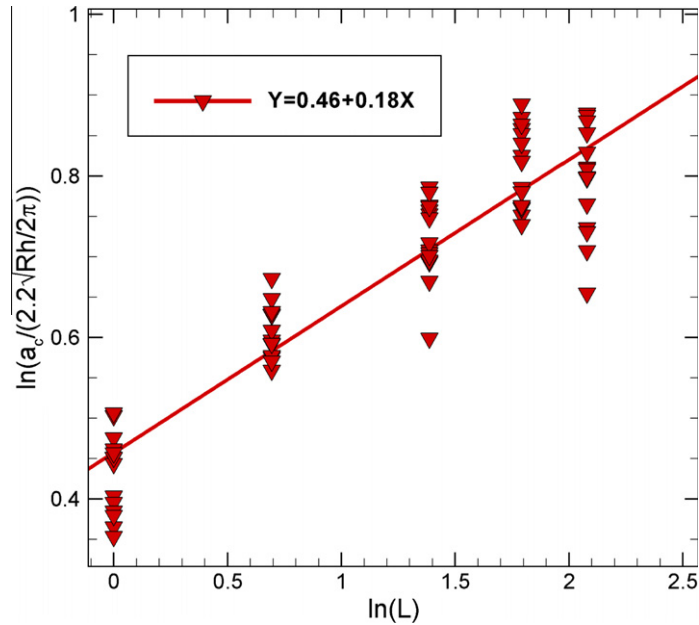


Fig. 9. The dependence of $\ln[a_c^e / (2.2\sqrt{Rh/2\pi})]$ on $\ln(L)$.

(2) Dislocation distribution underneath the indenter closely depends on the thin film thickness. In thinner films, in order to accommodate the applied indentation depth, some dislocations must nucleate and glide on those slip planes far from the central plane of the indenter; however, in thicker films, almost all dislocations nucleate and glide within a rectangular zone underneath the indenter. For both thin and thick films, most of the geometrically necessary dislocations reside within a rectangular zone with an area $A_{GND} = a_c L$, which is different from the assumption that all GNDs are stored in a hemispheroidal or semicircular zone (Swadener et al., 2001, 2002; Nix and Gao, 1998).

(3) Nano-indentation hardness not only depends on the indentation depth and indenter radius but also on the film thickness. A simple empirical model is proposed, which suggests a linear dependence of the square of the micro-hardness (H^2) on the square root of the ratio of the indentation depth to the indenter radius ($\sqrt{h/R}$) and an exponential dependence on the thin film thickness (L).

It should be pointed out, however, that in this contribution, only two-dimensional cases of plane strain are considered. Without any doubt, it is meaningful to extend the present analysis and model to more general three-dimensional cases. On the other hand,

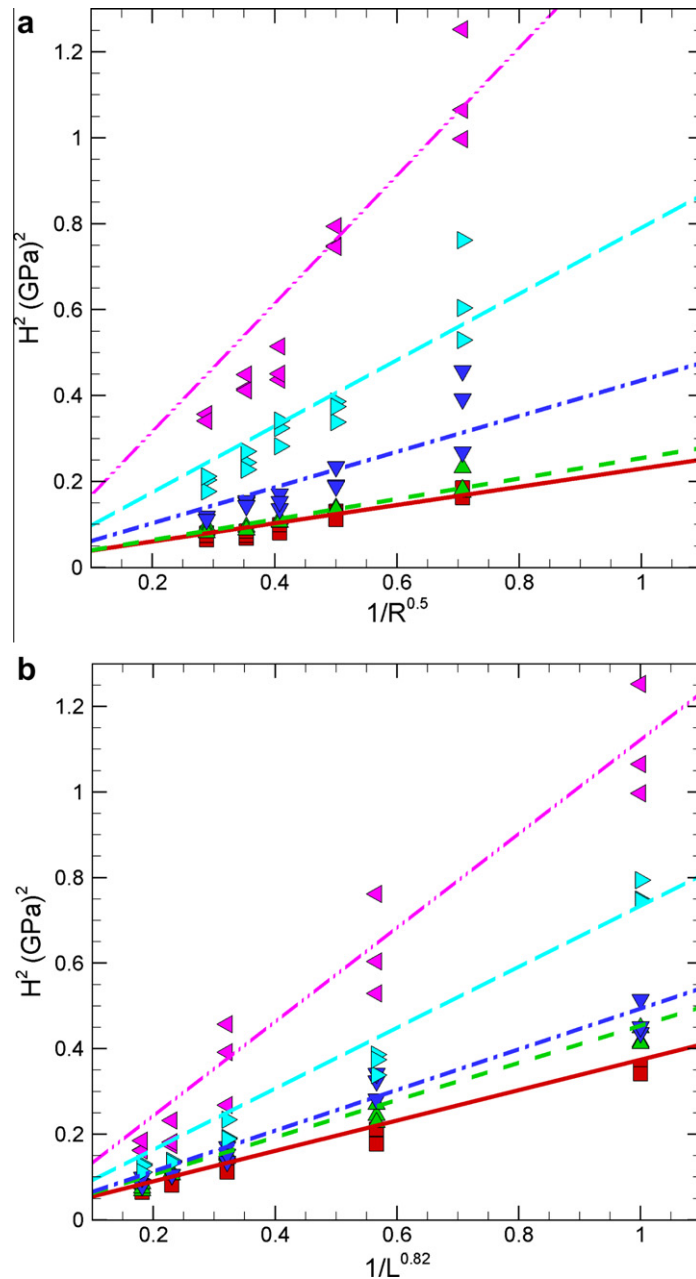


Fig. 10. Comparisons between model prediction and computing results for the variations of the square of indentation hardness H^2 with (a) $1/\sqrt{R}$ and (b) $1/L^{(1-\beta)}$ with $\beta = 0.18$.

although two or three slip systems also can be considered, only a simple single slip system is considered for simplicity. In addition, the elastic properties of the thin film and the substrate are taken as the same. In fact, the thin film may be softer or harder than the substrate. These questions need further discussions in detail.

Acknowledgments

Partial financial support from NSFC by grant 10672064 is acknowledged. We would like to express our heartfelt gratitude to anonymous reviewers for their helpful comments and suggestions.

References

Abu Al-Rub, R.K., 2007. Prediction of micro and nanoindentation size effect from conical or pyramidal indentation. *Mech. Mater.* 39, 787–802.

- Abu Al-Rub, R.K., Voyiadjis, G.Z., 2004. Analytical and experimental determination of the material intrinsic length scale of strain gradient plasticity theory from micro- and nano-indentation experiments. *Int. J. Plast.* 20, 1139–1182.
- Arsenlis, A., Parks, D.M., 1999. Crystallographic aspects of geometrically-necessary and statistically-stored dislocation density. *Acta Mater.* 47, 1597–1611.
- Balint, D.S., Deshpande, V.S., Needleman, A., Van der Giessen, E., 2006. Discrete dislocation plasticity analysis of the wedge indentation of films. *J. Mech. Phys. Solids* 54, 2281–2303.
- Bolesta, A.V., Fomin, V.M., 2009. Molecular dynamics simulation of sphere indentation in a thin copper film. *Phys. Mesomech.* 12, 117–123.
- Buckle, H., 1973. In: Westbrook, J.H., Conrad, H. (Eds.), *The Science of Hardness Testing and Its Research Applications*. American Society for Metals, Metals Park, Ohio, p. 453.
- Chen, S.H., Liu, L., Wang, T.C., 2005. Investigation of the mechanical properties of thin films by nanoindentation, considering the effects of thickness and different coating-substrate combinations. *Surf. Coat. Technol.* 191, 25–32.
- Chen, S.H., Liu, L., Wang, T.C., 2007. Small scale, grain size and substrate effects in nano-indentation experiment of film-substrate systems. *Int. J. Solids Struct.* 44, 4492–4504.
- Durst, K., Backes, B., Franke, O., Göken, M., 2006. Indentation size effect in metallic materials: Modeling strength from pop-in to macroscopic hardness using geometrically necessary dislocations. *Acta Mater.* 54, 2547–2555.

- Elmustafa, A.A., Stone, D.S., 2002. Indentation size effect in polycrystalline FCC metals. *Acta Mater.* 50, 3641–3650.
- Elmustafa, A.A., Ananda, A.A., Elmahboub, W.M., 2004. Dislocation mechanics simulations of the bilinear behavior in micro- and nanoindentation. *J. Mater. Res.* 19, 768–779.
- Espinosa, H.D., Prorok, B.C., Fischer, M., 2003. A methodology for determining mechanical properties of freestanding thin films and MEMS materials. *J. Mech. Phys. Solids* 51, 47–67.
- Feng, G., Nix, W.D., 2004. Indentation size effect in MgO. *Scr. Mater.* 51, 599–603.
- Fredriksson, P., Larsson, P.L., 2008. Wedge indentation of thin films modeled by strain gradient plasticity. *Int. J. Solids Struct.* 45, 5556–5566.
- Groh, S., Zbib, H.M., 2009. Advances in discrete dislocations dynamics and multiscale modeling. *J. Eng. Mater. Technol.* 131, 041209.
- Huang, Y., Zhang, F., Hwang, K.C., Nix, W.D., Pharr, G.M., Feng, G., 2006. A model of size effects in nano-indentation. *J. Mech. Phys. Solids* 54, 1668–1686.
- Huang, Y., Feng, X., Pharr, G.M., Hwang, K.C., 2007. A nano-indentation model for spherical indenters. *Model. Simul. Mater. Sci. Eng.* 15, S255–S262.
- Joslin, D.L., Oliver, W.C., 1990. A new method for analyzing data from continuous depth-sensing micro-indentation tests. *J. Mater. Res.* 5, 123–126.
- Kreuzer, H.G.M., Pippin, R., 2004. Discrete dislocation simulation of nanoindentation. *Comp. Mech.* 33, 292–298.
- Kreuzer, H.G.M., Pippin, R., 2007. Discrete dislocation simulation of nanoindentation: indentation size effect and the influence of slip band orientation. *Acta Mater.* 55, 3229–3235.
- Lim, Y.Y., Chaudhri, M.M., 1999. The effect of the indenter load on the nanohardness of ductile metals: an experimental study on polycrystalline work-hardened and annealed oxygen-free copper. *Philos. Mag.* A 79, 2979–3000.
- Liu, Y., Ngan, A.H.W., 2001. Depth dependence of hardness in copper single crystals measured by nanoindentation. *Scr. Mater.* 44, 237–241.
- Ma, Q., Clarke, D.R., 1995. Size dependent hardness of silver single crystals. *J. Mater. Res.* 10, 853–863.
- McElhaney, K.W., Vlassak, J.J., Nix, W.D., 1998. Determination of indenter tip geometry and indentation contact area for depth-sensing indentation experiments. *J. Mater. Res.* 13, 1300–1306.
- Nix, W.D., 1989. Mechanical properties of thin films. *Metall. Mater. Trans. A* 20, 2217–2245.
- Nix, W.D., Gao, H., 1998. Indentation size effects in crystalline materials: a law for strain gradient plasticity. *J. Mech. Phys. Solids* 46, 411–425.
- Oliver, W.C., Pharr, G.M., 2004. Measurement of hardness and elastic modulus by instrumented indentation: advances in understanding and refinements to methodology. *J. Mater. Res.* 19, 3–20.
- Olmsted, D.L., Hardikar, K.Y., Phillips, R., 2001. Lattice resistance and Peierls stress in finite size atomistic dislocation simulations. *Modell. Simul. Mater. Sci. Eng.* 9, 215–247.
- Ouyang, C., Li, Z., Huang, M., Hou, C., 2008. Discrete dislocation analyses of circular nanoindentation and its size dependence in polycrystals. *Acta Mater.* 56, 2706–2717.
- Pelletier, H., Krier, J., Mille, P., 2006. Characterization of mechanical properties of thin films using nanoindentation test. *Mech. Mater.* 38, 1182–1198.
- Qin, J., Qu, S., Feng, X., Huang, Y., Xiao, J., Hwang, K.C., 2009. A numerical study of indentation with small spherical indenters. *Acta Mech. Solida Sin.* 22, 18–26.
- Qiu, X., Huang, Y., Nix, W.D., Hwang, K.C., Gao, H., 2001. Effect of intrinsic lattice resistance in strain gradient plasticity. *Acta Mater.* 49, 3949–3958.
- Qu, S., Huang, Y., Pharr, G.M., Hwang, K.C., 2006. The indentation size effect in the spherical indentation of iridium: A study via the conventional theory of mechanism-based strain gradient plasticity. *Int. J. Plast.* 22, 1265–1286.
- Saha, R., Nix, W.D., 2002. Effects of the substrate on the determination of thin film mechanical properties by nanoindentation. *Acta Mater.* 50, 23–38.
- Saha, R., Xue, Z., Huang, Y., Nix, W.D., 2001. Indentation of a soft metal film on a hard substrate: strain gradient hardening effects. *J. Mech. Phys. Solids* 49, 1997–2014.
- Stölken, J.S., Evans, A.G., 1998. A microbend test method for measuring the plasticity length scale. *Acta Mater.* 46, 5109–5115.
- Swadener, J.G., Taljat, B., Pharr, G.M., 2001. Measurement of residual stress by load and depth sensing indentation with spherical indenters. *J. Mater. Res.* 16, 2091–2102.
- Swadener, J.G., George, E.P., Pharr, G.M., 2002. The correlation of the indentation size effect measured with indenters of various shapes. *J. Mech. Phys. Solids* 50, 681–694.
- Van der Giessen, E., Needleman, A., 1995. Discrete dislocation plasticity: a simple planar model. *Modell. Simul. Mater. Sci. Eng.* 3, 689–735.
- Vlassak, J., Nix, W.D., 1992. New bulge test technique for the determination of Young's modulus and Poisson's ratio of thin films. *J. Mater. Res.* 7, 3242–3249.
- Voyiadis, G., Deliktas, B., 2009. Theoretical and experimental characterization for the inelastic behavior of the micro-/nanostructured thin films using strain gradient plasticity with interface energy. *J. Eng. Mater. Technol.* 131, 041202.
- Widjaja, A., Van der Giessen, E., Needleman, A., 2005. Discrete dislocation modelling of submicron indentation. *Mater. Sci. Eng. A* 400, 456–459.
- Widjaja, A., Van der Giessen, E., Deshpande, V.S., Needleman, A., 2007a. Contact area and size effects in discrete dislocation modeling of wedge indentation. *J. Mater. Res.* 22 (3), 655–663.
- Widjaja, A., Van der Giessen, E., Needleman, A., 2007b. Discrete dislocation analysis of the wedge indentation of polycrystals. *Acta Mater.* 55, 6408–6415.
- Widjaja, A., Needleman, A., Van der Giessen, E., 2007c. The effect of indenter shape on sub-micron indentation according to discrete dislocation plasticity. *Modell. Simul. Mater. Sci. Eng.* 15, S121–S131.
- Xu, Z.H., Rowcliffe, D., 2004. Finite element analysis of substrate effects on indentation behaviour of thin films. *Thin Solid Films* 447, 399–405.
- Xue, Z., Huang, Y., Hwang, K.C., Li, M., 2002. The influence of indenter tip radius on the micro-indentation hardness. *J. Eng. Mater. Technol.* 124, 371–379.
- Zhang, T.Y., Xu, W.H., Zhao, M.H., 2004. The role of plastic deformation of rough surfaces in the size-dependent hardness. *Acta Mater.* 52, 57–68.
- Zhang, F., Saha, R., Huang, Y., Nix, W.D., Hwang, K.C., Qu, S., Li, M., 2007. Indentation of a hard film on a soft substrate: strain gradient hardening effects. *Int. J. Plast.* 23, 25–43.
- Zhao, M., Chen, X., Xiang, Y., Vlassak, J.J., Lee, D., Ogasawara, N., Chiba, N., Gan, Y.X., 2007. Measuring elastoplastic properties of thin films on an elastic substrate using sharp indentation. *Acta Mater.* 55, 6260–6274.
- Zhao, M., Xiang, Y., Xu, J., Ogasawara, N., Chiba, N., Chen, X., 2008. Determining mechanical properties of thin films from the loading curve of nanoindentation testing. *Thin Solid Films* 516, 7571–7580.